ACS Partner Journal
PRECISION CHEMISTRY

pubs.acs.org/PrecisionChem
Article

A General Synthesis Method for Covalent Organic Framework and Inorganic 2D Materials Hybrids

Yifan Zhu, Yunrui Yan, Yuren Feng, Yifeng Liu, Chen-Yang Lin, Qing Ai, Tianshu Zhai, Bongki Shin, Rui Xu, Hongchen Shen, Qiyi Fang, Xiang Zhang, Dayanni Bhagwandin, Yimo Han, Hanyu Zhu, Nicholas R. Glavin, Pulickel M Ajayan, Qilin Li, and Jun Lou*

Cite This: *Precis. Chem.* 2024, 2, 398−405
Read Online

ACCESS | Metrics & More | Article Recommendations | Supporting Information

ABSTRACT: Two-dimensional (2D) inorganic/organic hybrids provide a versatile platform for diverse applications, including electronic, catalysis, and energy storage devices. The recent surge in 2D covalent organic frameworks (COFs) has introduced an organic counterpart for the development of advanced 2D organic/inorganic hybrids with improved electronic coupling, charge separation, and carrier mobility. However, existing synthesis methods have primarily focused on few-layered film structures, which limits scalability for practical applications. Herein, we present a general synthesis approach for a range of COF/inorganic 2D material hybrids, utilizing 2D inorganic materials as both catalysts and inorganic building blocks. By leveraging the intrinsic Lewis acid sites on the inorganic 2D materials such as hexagonal boron nitride (hBN) and transition metal dichalcogenides, COFs with diverse functional groups and topologies can grow on the surface of inorganic 2D materials. The controlled 2D morphology and excellent solution dispersibility of the resulting hybrids allow for easy processing into films through vacuum filtration. As proof of concept, hBN/COF films were employed as filters for Rhodamine 6G removal under flow-through conditions, achieving a removal rate exceeding 93%. The present work provides a simple and versatile synthesis method for the scalable fabrication of COF/inorganic 2D hybrids, offering exciting opportunities for practical applications such as water treatment and energy storage.

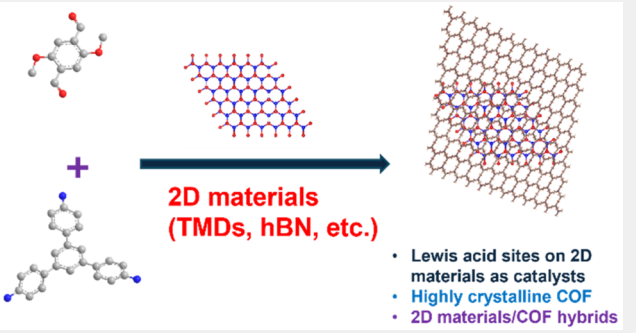

KEYWORDS: *Covalent organic frameworks, Transition-metal dichalcogenides, Lewis acid catalysts, Hexagonal boron nitride, Hybrid Materials*

INTRODUCTION

Two-dimensional (2D) inorganic/organic hybrids provide a versatile platform for a wide range of applications, encompassing electronic, catalysis, and energy storage devices.[1−8] The combination of 2D inorganic materials like transition metal dichalcogenides (TMDs) and hexagonal boron nitride (hBN) with an extensive assortment of organic molecules and polymers undeniably extends the frontiers of a novel family of organic/inorganic heterostructures.[2,9] This approach allows for the synergistic integration of the strengths of both material classes while mitigating their respective limitations.[2] The rich library of organic materials provides a large degree of freedom for chemical tunability to the 2D inorganic crystals. Moreover, deliberate selection of organic semiconductors to achieve aligned energy band and well-bonded interfaces with inorganic 2D semiconductors facilitates charge carrier transfer and migration in electronic devices,[10] consequently boosting the device performance.[2,4] Hence, there is a widespread interest in developing novel 2D inorganic/organic hybrids.

Covalent organic frameworks (COFs) are an emerging class of 2D polymers known for their tunable structures, remarkable stability, and extensive surface areas,[11−13] making them invaluable in applications such as pollutant removal,[14−16] energy storage,[17,18] catalysis,[19−22] biomedicine,[23] and others.[24−26] Recent advancements demonstrate that combining COFs with inorganic 2D materials forms hybrid structures and devices with improved electronic coupling, charge separation, and carrier mobility,[27−29] offering significant potential in optoelectronic device development.[8,30−32] The previously reported synthesis methods for COFs/2D inorganic hybrids, such as direct growth,[32] layer-by-layer transfer,[30] and microwave-facilitated deposition,[27] have primarily concentrated on producing a few-layered 2D structures with thin film configurations. However, the challenge lies in scaling up

Special Issue: Precision Chemistry for Two-Dimensional Materials

Received: December 16, 2023
Revised: April 25, 2024
Accepted: April 26, 2024
Published: May 2, 2024

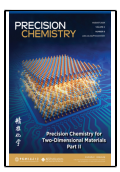

https://doi.org/10.1021/prechem.3c00118
Precis. Chem. 2024, 2, 398−405

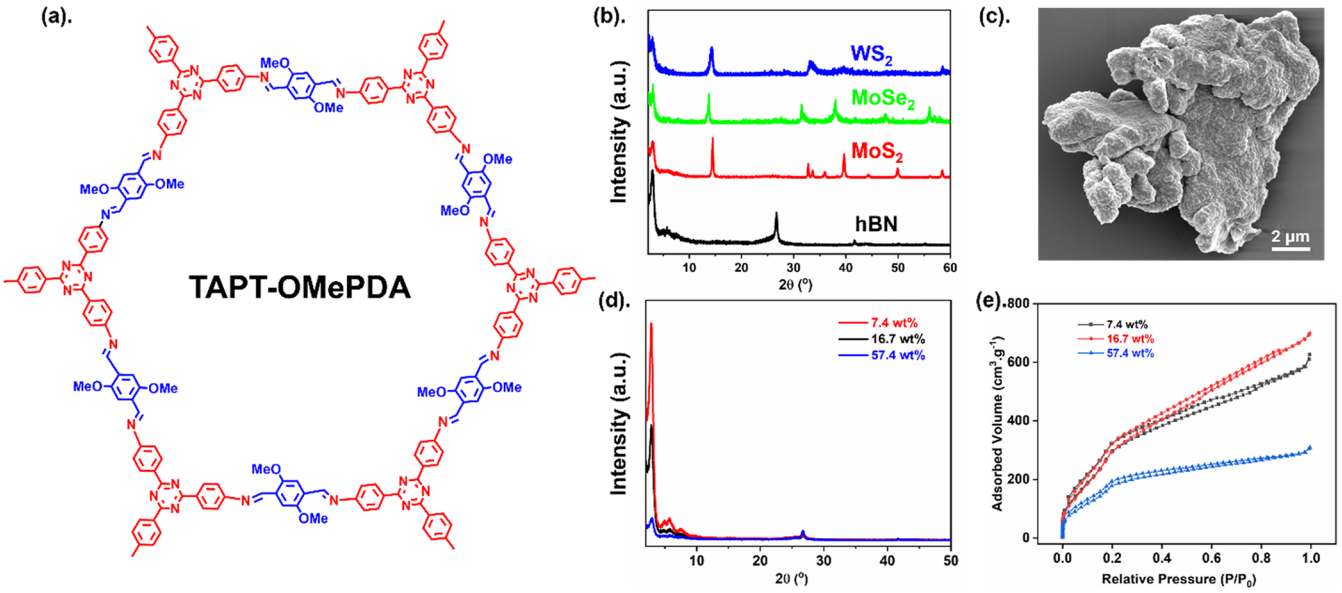

Figure 1. (a) Structure of TAPT-OMePDA COF. (b) PXRD of different 2D materials/TAPT-OMePDA hybrids using 57.4 wt % 2D materials. (c) SEM of hBN/TAPT-OMePDA hybrids synthesized using 57.4 wt % hBN. (d) PXRD of hBN/TAPT-OMePDA hybrids catalyzed by different hBN ratios. (e) BET isotherms of different hBN/TAPT-OMePDA hybrids with different hBN ratio.

these methods, limiting their applicability in areas like gas separation, water treatment, and batteries, where large-scale, solution-processable multilayer 2D nanosheets are typically needed.[33,34] Therefore, it is imperative to develop general synthetic methodologies for producing large scale COF/inorganic hybrids while preserving their 2D morphology and solution processability.

Recent research has demonstrated that Lewis acids can effectively catalyze the synthesis of imine COFs with high crystallinity.[35−38] By leveraging the analogous Lewis acidity found in 2D inorganic materials like hBN[39] and TMDs,[40] we postulated that these materials could function as both catalysts and inorganic building blocks for creating COF/inorganic hybrids, enabling the controlled growth of COFs on the surface of such 2D materials. Herein, we present a general synthetic method for a series of COF/inorganic 2D material hybrids, catalyzed by various inorganic 2D materials, including hBN, molybdenum disulfide (MoS_2), molybdenum diselenide ($MoSe_2$), and tungsten disulfide (WS_2). This approach enables the growth of a diverse range of imine-based COFs with varying functional groups and topologies at the interface of 2D inorganic building blocks, resulting in COF/inorganic hybrids featuring high crystallinity and a large surface area. Through the careful control of COF monomers and inorganic 2D component concentrations, these COF/inorganic 2D material hybrids maintain controlled 2D morphology and good solution dispersity, allowing for easy processing into thin films via the vacuum filtration method. As a proof of concept, we employed COF/hBN films as filters for the removal of organic dyes under flow-through conditions. This straightforward yet versatile synthesis method significantly reduces barriers to scalable COF/inorganic 2D hybrid material synthesis, unlocking numerous possibilities for practical applications such as water treatment and energy storage.

RESULTS AND DISCUSSION

We first evaluated the potential of using the surface of 2D materials to catalyze COF growth, resulting in the controllable formation of COF/inorganic 2D materials heterostructures. The 2D materials explored in this study included ball-milled hBN and TMDs (MoS_2, $MoSe_2$, WS_2, Scheme S1) with 2,4,6-tris(4-aminophenyl)-1,3,5-triazine (TAPT) and 2,5-dimethoxyterephthaldehyde (OMePDA) employed as model monomers for COF (TAPT-OMePDA, Figure 1a) formation. The loading ratio of 2D materials was 57.4 wt % relative to the total weight of COF monomers, with a concentration of 15 mg/mL. The polycondensation reaction was carried out under 120 °C for 3 days using a mixture of 1,4-dioxane and mesitylene in a 1:1 volume ratio. As anticipated, yellowish, insoluble solid precipitation was obtained. The obtained products exhibited excellent crystallinity, as evidenced by the distinct and prominent powder X-ray diffraction (PXRD) patterns from both COFs and 2D materials (Figure 1b). For example, in the hBN/COF heterostructure, the peaks centered at 27.5° and 43.5° were attributed to the (100) and (110) facets of hBN,[41] respectively, while peaks at smaller angles 2.8°, 4.8°, 5.9°, and 7.8°, corresponded to the (100), (110), (200), and (210) facets of crystalline TAPB-OMePDA COF,[37] respectively. Similar successful COF formation were observed for other types of TMD materials (Figure 1b), indicating their potential as effective catalysts. It is worth noting that the PXRD patterns of the TMD-catalyzed COFs displayed broader peaks compared to the h-BN catalyzed COFs, suggesting smaller crystal domains.[42] Fourier-transform infrared (FT-IR) spectroscopy further confirmed the successful condensation of aldehyde and amine moieties by the presence of C═N stretching at around 1615 cm^{-1} (Figures S1−S4), indicating the formation of imine bonds during the condensation reaction. Thermogravimetric analysis (TGA) of the hBN/COF samples revealed that the TAPT-OMePDA COF exhibited thermal stability up to 400 °C (Figure S5), which aligns well with previous findings that employed acetic acid as the catalyst.[43] Additionally, the hBN content in the composites was determined to be approximately 41.2% via TGA (Figure S5). Morphological characterization of the initial 2D materials and resulting heterostructures was performed using scanning

https://doi.org/10.1021/prechem.3c00118
Precis. Chem. 2024, 2, 398−405

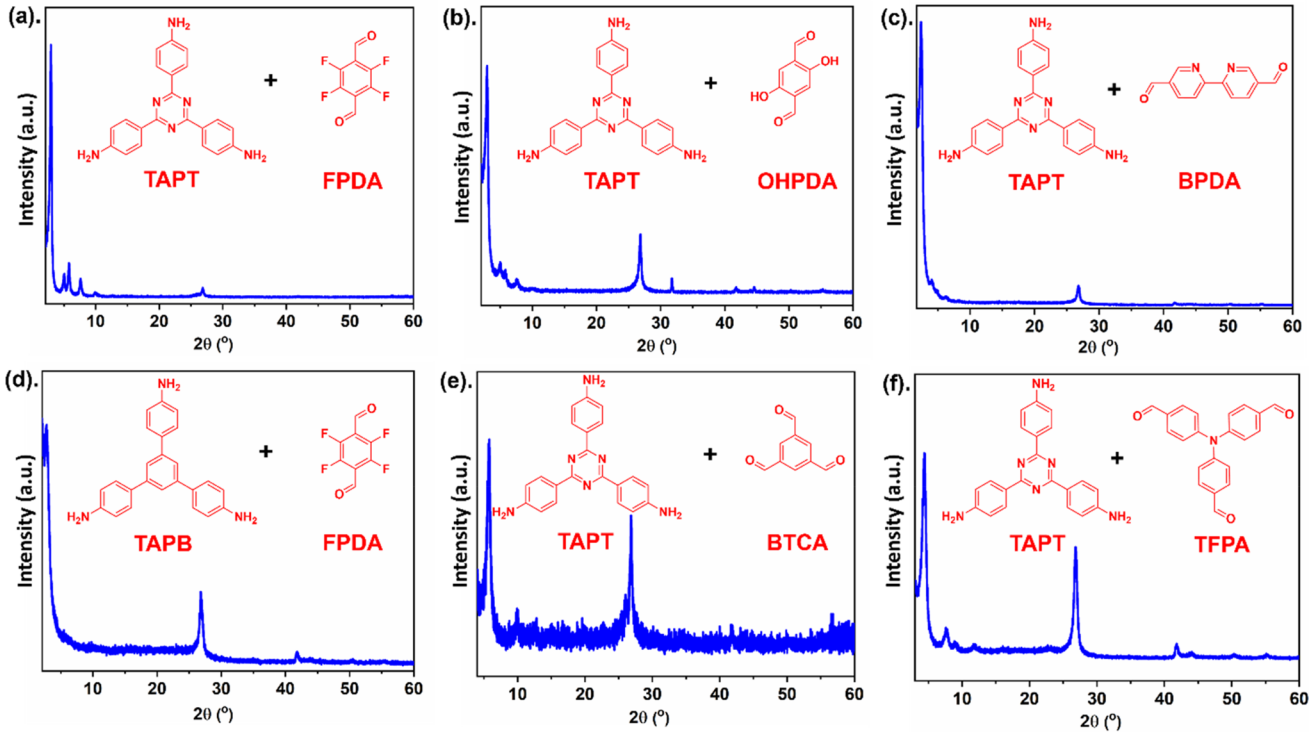

Figure 2. PXRD spectra of (a) hBN/TAPT-FPDA hybrids, (b) hBN/TAPT−OHPDA hybrids, (c) hBN/TAPT-BPDA hybrids, (d) hBN/TAPB-FPDA hybrids, (e) hBN/TAPT-BTCA hybrids, and (f) hBN/TAPT-TFPA hybrids. FPDA = 2,3,5,6-tetrafluoroterephthalaldehyde; OHPDA = 2,5-dihydroxy-1,4-benzenedicarboxaldehyde; BPDA = 5,5′-dialdehyde-2,2′-bipyridine; TAPB = 1,3,5-tris(4-aminophenyl) benzene; BTCA = benzene-1,3,5-tricarbaldehyde; TFPA = tris(4-formylphenyl)amine. hBN/COF hybrids were synthesized using 57.4 wt % hBN as the catalyst.

electron microscopy (SEM, Figures 1c, S6−S12). The SEM imaging of hBN/COF hybrids revealed sheetlike structures derived from hBN, featuring a rough surface attributed to aggregated COF particles (Figure 1c). In contrast, pure hBN sheets exhibited smooth surfaces (**Figure S9**). Similar morphological features were consistently observed in other TMD/COFs heterostructures (**Figures S6−S8**). Ball milled hBN was selected as the representative example for further investigation due to the superior crystallinity exhibited by the resulting composites. We propose that through Lewis acid−base interaction, the electron-rich oxygen in the aldehyde coordinates with Lewis acid sites on TMD/hBN,[44] rendering the carbonyl carbons more electrophilic and facilitating nucleophilic attack by amine groups.[35,37] This interaction was further revealed by the FT-IR analysis. Examination of the FT-IR spectra of the OMePDA monomer and MoS_2-OMePDA (**Figure S13**) complex showed that the peak at 1669 cm^{-1}, corresponding to the C═O stretching of the aldehyde group in OMePDA, shifted to 1675 cm^{-1} in the MoS_2-OMePDA complex and significantly broadened, indicating possible Lewis acid−base coordination.[45] The detailed proposed mechanism of imine COF formation is depicted in Scheme S2.

Additionally, we explored the impact of surface defects in 2D materials on the fabrication of such composites. To accomplish this, hBN flakes were ball-milled prior to exposure to the monomers, as the ball-milling process has been shown to introduce more surface defects and provides more active areas for hBN due to shear force exfoliation.[41] As expected, the isolated yield of the COF/hbN composites using ball-milled hBN (80.6%) was significantly higher than that of pristine hBN (43.7%). The PXRD of both composites exhibited prominent peaks located at 2.8° and 27.5° that corresponds to COF and hBN, respectively (**Figure S14**). These results indicate the potential of using defects and surface engineering to tune the crystallinity and increase the yield of COFs, highlighting the versatility of 2D materials as catalysts. A more detailed investigation into the impact of surface defects will be addressed in the forthcoming study.

Next, we investigated how the ratio of 2D materials used influences the crystallinity and yield of the resulting composites. As depicted in Figure 1d, with a reduced hBN ratio, the PXRD patterns of the COF component in the composites exhibited sharpened peaks and increased intensity. For instance, the full width at half-maximum (FWHM) of the peak at 2.8° decreased from 1.3° to 0.90° to 0.75° as the catalysis ratio decreased from 57.4 wt % to 16.7 wt % to 7.4 wt %. This reduction in FWHM indicates an increase in crystal domain size, implying an enhancement in the crystallinity of the resulting COFs.[42] The decreased crystallinity of COFs in the composites is expected to be due to the excess amount of Lewis acid present at higher hBN ratios, which could suppress the imine exchange during the polycondensation process.[35] Moreover, the Brunauer−Emmett−Teller (BET) surface area of the composites was determined to be 1302 m^2/g, 1309 m^2/g, and 740 m^2/g for hBN ratios of 7.4, 16.7, and 57.4 wt %, respectively, using nitrogen sorption isotherms (Figure 1e). The pore size distribution of all composites is located at around 3.0−3.2 nm, which matched well with that of TAPT-OMePDA COF (**Figures S15−S17**).[46] The decreased surface area observed at 57.4 wt % hBN ratios is possibly due to the nonporous nature of hBN, which minimizes the overall surface area of the composites.[46,47] The hBN/COF hybrids were also observed in SEM in the cases of using 7.4 and 16.7 wt % hBN

https://doi.org/10.1021/prechem.3c00118
Precis. Chem. 2024, 2, 398−405

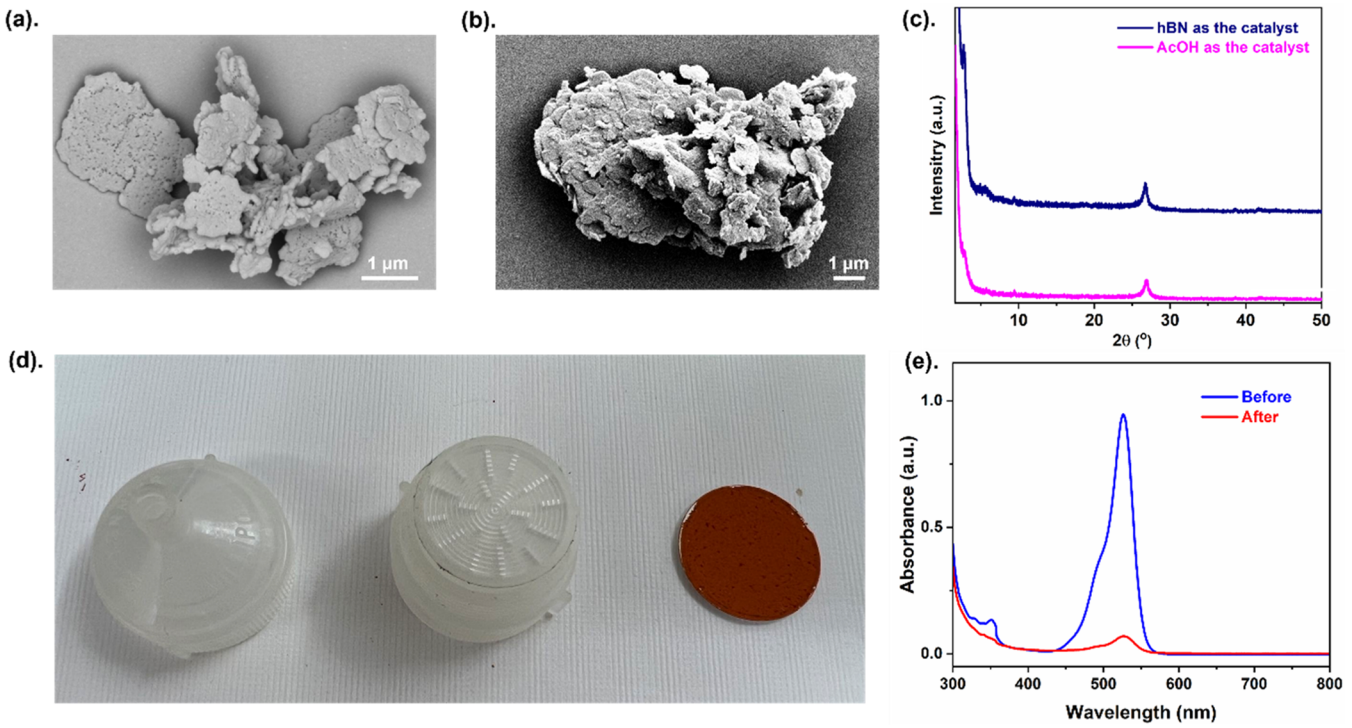

Figure 3. (a) SEM images of hBN/TAPT-FPDA sheets using 1 mg/mL hBN, 0.008 mmol/mL TAPT, and 0.012 mmol/mL of FPDA. (b) SEM images of hBN/TAPT-FPDA synthesized with the using AcOH as catalyst. Other reaction conditions are the same as those in Figure 3a. (c) PXRD of hBN/TAPT-FPDA obtained with and without AcOH catalyst. (d) Pictures of the syringe filter and hBN/TAPT-OHPDA loaded membrane obtained via vacuum filtration. (e) UV−vis spectra of Rhodamine 6G before (blue) and after (red) flowing through the hBN/TAPT-OHPDA filter.

as catalysts (**Figures S18−S19**). It is worth noting that in the produced composites from using 7.4 wt % of hBN, some hybrids did not exhibit a sheetlike structure but were completely covered by COFs (**Figure S19b**). This phenomenon may be attributed to the relatively low ratio of hBN compared to the COFs.

To comprehensively understand the generality of 2D materials in promoting the synthesis of 2D material/COF hybrids, we conducted a broader exploration by using different monomers to generate COFs with diverse functional groups, topologies, and pore sizes (Figure 2). Encouragingly, the inert hBN flakes demonstrated excellent tolerance to other substituted functional groups (−F, −OH) and pyridine-based aldehyde monomers. The PXRD patterns of the resulting products exhibited prominent and narrow peaks, consistent with previous studies,[35,37,42,48−50] indicating the successful formation of high-crystalline COFs. Moreover, we achieved considerable composite yields in all cases, with 86.5% for TAPT-FPDA, 87.3% for TAPT−OHPDA, and 87.3% for TAPT-BPDA (Figures 2a−c). Furthermore, when we replaced the amine monomer with a TAPB-based backbone, successful COF formation was still obtained in the case of TAPB-FPDA and TAPB-PDA, as evidenced by the PXRD patterns (Figure 2d and **Figure S20**). Notably, we also investigated different node-linker topologies, such as the "3 + 3" configuration and found that hBN effectively catalyzed the synthesis of TAPT-BTCA and TAPT-TFPA COFs with yields of 75.7% and 80.5%, respectively. PXRD analysis further verified good crystallinity of both COFs (Figures 2e, f).[51,52] The COFs synthesized using different monomers exhibited a diverse range of pore sizes, spanning from 1.45 nm for TAPT-BTCA[52] to 4.0 nm for TAPT-BPDA.[53] These findings unequivocally demonstrate the remarkable versatility and efficacy of 2D hBNs in catalyzing the formation of hBN/COF hybrids with tunable properties.

Despite the successful formation of heterojunctions, the resulting composites lost their original sheetlike structure from the 2D materials and instead exhibited an aggregated lump morphology from SEM (e.g., Figure 1c for TAPT-OMePDA, **Figure S21** for TAPT-FPDA). These aggregated composites showed poor dispersity and were difficult to process, which hindered their further use in membrane and thin film devices.[8] We hypothesized that the aggregation might arise from two factors: (1) a high concentration of 2D materials leading to the tendency of 2D materials themselves to aggregate before polymerization commences[54] and (2) an excessively fast polymerization rate due to high monomer concentration, resulting in early stage polymerization-induced phase segregation and interparticle cross-linking.[55] The polymerization rate is governed by concentration of both monomers and catalysts.[46,55,56] To overcome this challenge,[54] we employed a low initial concentration of 2D materials (1 mg/mL) to prevent their aggregation. TAPT-FPDA was selected as the targeted COF due to its outstanding crystallinity (Figure 2a). The monomer concentrations of TAPT and FPDA were reduced to 0.008 mmol/mL and 0.012 mmol/mL, respectively. The reduced concentration of both the monomers and 2D materials helped to avoid cross-linking between nanosheets and prevented COF particles from detaching from the 2D materials due to adsorption−desorption equilibrium. Instead, it enabled the COFs to grow on the surface of the 2D materials.[57] As anticipated, yellowish solids can be observed after 4 h at 120 °C under hydrothermal conditions. Subsequently, following an additional 68 h under the same conditions, a yellowish hBN/TAPT-FPDA heterostructure was successfully obtained. SEM images (Figure 3a) revealed that

https://doi.org/10.1021/prechem.3c00118
Precis. Chem. 2024, 2, 398−405

the heterostructure retained the sheetlike structure of hBN without significant aggregation, while exhibiting a rough and porous coating corresponding to the COFs. Transmission electron microscopy (TEM) analysis (Figure S22) displayed the presence of a COF layer also coated on the hBN edge. FT-IR spectra exhibited characteristic peaks at 1606 cm^{-1} (Figure S23), corresponding to the C═N stretching of imine moieties in TAPT-FPDA. Furthermore, the transmission spectra (Figure S24) showed a prominent absorption edge at around 510 nm corresponding to the optical gap of TAPT-FPDA.[58] Importantly, no such characteristic feature was evident in the transmission spectra of hBN. Collectively, the above evidence confirms the successful formation of COFs on the hBN surface. As a control experiment, hBN/TAPT-FPDA hybrids were grown under the same conditions but with the additional introduction of 6 M AcOH. Upon adding AcOH, yellow solids rapidly formed and precipitated, which is presumably due to fast and uncontrollable polymerization rate, leading to the formation of large COF clusters.[59] After 72 h under these conditions, the hBN/TAPT-FPDA structure exhibited nonuniform coating of COFs on hBN and aggregated features, as shown in Figure 3b and Figure S25. This contrasted with the controlled morphology achieved when using only hBN as the catalyst (Figure 3a). Furthermore, the hBN/TAPT-FPDA resulted from employing hBN as the sole catalyst, displaying moderate crystallinity of COFs in PXRD (Figure 3c). In contrast, hBN/TAPT-FPDA prepared with AcOH showed a broad shoulder peak around 2.8° (Figure 3c), indicating relatively poor crystallinity. This could be attributed to the excessive presence of acid catalysts as both AcOH and hBN can serve as catalysts, which suppress the imine exchange process.[35,59] This comparison highlights hBN's remarkable capacity as a solid support/template catalyst to generate hBN/TAPT-FPDA composites with a more controllable morphology and superior crystallinity when compared to reactions catalyzed by AcOH.

Leveraging the controlled 2D morphology and excellent solution dispersibility of hBN/COFs hybrids, we proceeded to fabricate the hBN/TAPT-OHPDA film by employing vacuum filtration of the dispersed hybrid solution. The selection of TAPT-OHPDA COF was motivated by its hydrophilic nature,[49] which facilitates water flux. Unlike COF particles synthesized via traditional hydrothermal methods, which can be challenging to process,[8] the hBN/TAPT-OHPDA hybrids could be readily dispersed, forming a film supported by commercially available microfiltration membranes (Figure 3d). This streamlined process significantly simplifies the production of COF films, enabling their seamless integration onto the plastic filters (Figure 3d). This, in turn, allows for the efficient removal of organic contaminants when water flows through. As proof of concept, a solution containing 10 μmol L^{-1} Rhodamine 6G was pushed through syringe filters with hBN/TAPT-OHPDA film-loaded membranes at a rate of 0.5 mL s^{-1}. Encouragingly, the hBN/TAPT-OHPDA filter achieved an impressive 93% removal of Rhodamine 6G (Figure 3e), highlighting the robust capabilities of hBN/COF hybrids in effectively eliminating organic contaminants. In comparison, control experiments using films made from pure hBN and COF powders for dye removal showed lower efficiency (Figures S26−S27), with pure hBN and COF powders exhibiting 34.2% and 25.5% removal efficiency, respectively. The improved performance of 2D hybrids may stem from their dense stacking of 2D sheets, providing a longer distance and larger area for pollutant water to contact the adsorbents compared to particle stacking with pure COF. Additionally, films formed by isolated COF powders were prone to scratching off during the backwash process (Figure S28), attributable to their weak mechanical properties resulting from particle stacking.[55] The recycling ability of hBN/TAPT-OHPDA film for pollutant removal was further examined, demonstrating consistent removal performance over three cycles, maintaining removal rates from 91.2% to 92.2% (Figure S29). After backwash with DI water, nearly all rejected dye molecules were recovered in the backwashed water, exhibiting 89.9% to 91.7% dye recovery compared to the initial 10 μmol L^{-1} dye concentration (Figures S30−S31). The near 100% dye mass balance (Figure S31), achieved by adding filtered solution and backwash water, further confirms the good recycling ability.

CONCLUSION

In summary, our work introduces a versatile general synthesis method for a family of COF/inorganic 2D material hybrids, leveraging a variety of inorganic 2D materials as both catalysts and inorganic building blocks, including hBN, MoS_2, $MoSe_2$, and WS_2. This methodology facilitates the growth of diverse imine-based COFs with varying functional groups and topologies on the surface of 2D inorganic building blocks, yielding COF/inorganic hybrids featuring high crystallinity and substantial surface areas. By carefully adjusting the concentrations of COF monomers and inorganic 2D components, we obtain hybrids that maintain original 2D morphology with good solution dispersity, allowing for straightforward processing into thin films using vacuum filtration method. The COF/hBN films were then employed as filters for Rhodamine 6G removal under flow-through conditions, achieving more than 93% removal rate, which underscores their significant potential for the fabrication of membranes and thin film devices. This streamlined yet adaptable synthesis method effectively lowers the barriers to synthesize COF/inorganic 2D material hybrids, unveiling a wealth of possibilities for practical applications, particularly in water treatment and energy storage areas.

ASSOCIATED CONTENT

Supporting Information

The Supporting Information is available free of charge at https://pubs.acs.org/doi/10.1021/prechem.3c00118.

Materials and methods, experimental details, mechanism scheme and additional characterization data including PXRD, FT-IR, nitrogen sorption tests, TEM, TGA, and SEM (PDF)

AUTHOR INFORMATION

Corresponding Author

Jun Lou − *Department of Materials Science and Nanoengineering, Rice University, Houston, Texas 77005, United States; NSF Nanosystems Engineering Research Center Nanotechnology-Enabled Water Treatment, Rice University, Houston, Texas 77005, United States; Department of Chemistry, Rice University, Houston, Texas 77005, United States;* orcid.org/0000-0002-4351-9561; Email: jlou@rice.edu

https://doi.org/10.1021/prechem.3c00118
Precis. Chem. 2024, 2, 398−405

Authors

Yifan Zhu − *Department of Materials Science and Nanoengineering, Rice University, Houston, Texas 77005, United States;* orcid.org/0000-0002-9816-5764

Yunrui Yan − *Department of Materials Science and Nanoengineering, Rice University, Houston, Texas 77005, United States*

Yuren Feng − *Department of Civil and Environmental Engineering, Rice University, Houston, Texas 77005, United States; NSF Nanosystems Engineering Research Center Nanotechnology-Enabled Water Treatment, Rice University, Houston, Texas 77005, United States*

Yifeng Liu − *Department of Materials Science and Nanoengineering, Rice University, Houston, Texas 77005, United States*

Chen-Yang Lin − *Department of Materials Science and Nanoengineering, Rice University, Houston, Texas 77005, United States*

Qing Ai − *Department of Materials Science and Nanoengineering, Rice University, Houston, Texas 77005, United States;* orcid.org/0000-0002-6086-5431

Tianshu Zhai − *Department of Materials Science and Nanoengineering, Rice University, Houston, Texas 77005, United States*

Bongki Shin − *Department of Materials Science and Nanoengineering, Rice University, Houston, Texas 77005, United States*

Rui Xu − *Department of Materials Science and Nanoengineering, Rice University, Houston, Texas 77005, United States;* orcid.org/0000-0002-7072-1976

Hongchen Shen − *Department of Civil and Environmental Engineering, Rice University, Houston, Texas 77005, United States; NSF Nanosystems Engineering Research Center Nanotechnology-Enabled Water Treatment, Rice University, Houston, Texas 77005, United States*

Qiyi Fang − *Department of Materials Science and Nanoengineering, Rice University, Houston, Texas 77005, United States*

Xiang Zhang − *Department of Materials Science and Nanoengineering, Rice University, Houston, Texas 77005, United States;* orcid.org/0000-0003-4004-5185

Dayanni Bhagwandin − *UES, Inc., Beavercreek, Ohio 45432, United States; Materials and Manufacturing Directorate, Air Force Research Laboratory, Wright-Patterson AFB, Ohio 45433, United States*

Yimo Han − *Department of Materials Science and Nanoengineering, Rice University, Houston, Texas 77005, United States;* orcid.org/0000-0003-0563-4611

Hanyu Zhu − *Department of Materials Science and Nanoengineering, Rice University, Houston, Texas 77005, United States;* orcid.org/0000-0003-3376-5352

Nicholas R. Glavin − *Materials and Manufacturing Directorate, Air Force Research Laboratory, Wright-Patterson AFB, Ohio 45433, United States*

Pulickel M Ajayan − *Department of Materials Science and Nanoengineering, Rice University, Houston, Texas 77005, United States; Department of Chemistry, Rice University, Houston, Texas 77005, United States;* orcid.org/0000-0001-8323-7860

Qilin Li − *Department of Civil and Environmental Engineering, Rice University, Houston, Texas 77005, United States; NSF Nanosystems Engineering Research Center Nanotechnology-Enabled Water Treatment, Rice University, Houston, Texas 77005, United States;* orcid.org/0000-0001-5756-3873

Complete contact information is available at: https://pubs.acs.org/10.1021/prechem.3c00118

Author Contributions

Y.Z., Y.Y., and Y.F. contributed equally to this work. Y.Z., Y.Y., and J.L. designed and conceptualized the research. Y.Z., Y.Y., Y.L., Y. F., C. L., Q. A., T. Z., B.S., Q. F., H.S., R.X., and X. Z. performed the materials synthesis and characterization. All authors analyzed the data and discussed the results. Y.Z., Y.Y., Y.M., P.J.A, D.B., N.G., Q.L., and J.L. wrote and revised the paper. J.L. supervised the whole project.

Notes

The authors declare no competing financial interest.

■ ACKNOWLEDGMENTS

This work was supported by the Welch Foundation Grant C-1716, the NSF I/UCRC Center for Atomically Thin Multifunctional Coatings (ATOMIC) (EEC-2113882), and the NSF ERC on Nanotechnology-Enabled Water Treatment (EEC-1449500). B.S. and Y.H. acknowledge Welch under C-2065. The authors also acknowledge Shared Equipment Authority at Rice University for access and utilization of characterization instrumentation and the use of the Electron Microscopy Center (EMC) at Rice University. We thank Dr. Zhiwei Fang for the useful discussion. Y.Z. (Class of 2012, School of Gifted Young) and X.Z. (Class of 2009, School of Gifted Young) would like to express their heartfelt gratitude for the exceptional education they received at the University of Science and Technology of China (USTC).

■ REFERENCES

(1) Pham, P. V.; Bodepudi, S. C.; Shehzad, K.; Liu, Y.; Xu, Y.; Yu, B.; Duan, X. 2D Heterostructures for Ubiquitous Electronics and Optoelectronics: Principles, Opportunities, and Challenges. *Chem. Rev.* **2022**, *122* (6), 6514−6613.

(2) Xu, X.; Lou, Z.; Cheng, S.; Chow, P. C. Y.; Koch, N.; Cheng, H. M. Van Der Waals Organic/Inorganic Heterostructures in the Two-Dimensional Limit. *Chem.* **2021**, *7* (11), 2989−3026.

(3) Sun, J.; Choi, Y.; Choi, Y. J.; Kim, S.; Park, J.; Lee, S.; Cho, J. H. 2D-Organic Hybrid Heterostructures for Optoelectronic Applications. *Adv. Mater.* **2019**, *31* (34), 1803831.

(4) Pei, K.; Zhai, T. Emerging 2D Organic-Inorganic Hetero-junctions. *Cell Rep. Phys. Sci.* **2020**, *1* (8), 100166.

(5) Liu, Y.; Weiss, N. O.; Duan, X.; Cheng, H. C.; Huang, Y.; Duan, X. Van Der Waals Heterostructures and Devices. *Nature Reviews Materials 2016 1:9* **2016**, *1* (9), 1−17.

(6) Xiong, P.; Wu, Y.; Liu, Y.; Ma, R.; Sasaki, T.; Wang, X.; Zhu, J. Two-Dimensional Organic-Inorganic Superlattice-like Heterostructures for Energy Storage Applications. *Energy Environ. Sci.* **2020**, *13* (12), 4834−4853.

(7) Azadmanjiri, J.; Wang, J.; Berndt, C. C.; Yu, A. 2D Layered Organic-Inorganic Heterostructures for Clean Energy Applications. *J. Mater. Chem. A Mater.* **2018**, *6* (9), 3824−3849.

(8) Beagle, L. K.; Fang, Q.; Tran, L. D.; Baldwin, L. A.; Muratore, C.; Lou, J.; Glavin, N. R. Synthesis and Tailored Properties of Covalent Organic Framework Thin Films and Heterostructures. *Mater. Today* **2021**, *51*, 427−448.

(9) Gobbi, M.; Orgiu, E.; Samorì, P. When 2D Materials Meet Molecules: Opportunities and Challenges of Hybrid Organic/Inorganic van Der Waals Heterostructures. *Adv. Mater.* **2018**, *30* (18), 1706103.

(10) Choi, J.; Zhang, H.; Choi, J. H. Modulating Optoelectronic Properties of Two-Dimensional Transition Metal Dichalcogenide Semiconductors by Photoinduced Charge Transfer. *ACS Nano* **2016**, *10* (1), 1671−1680.
(11) Côté, A. P.; Benin, A. I.; Ockwig, N. W.; O'Keeffe, M.; Matzger, A. J.; Yaghi, O. M. Porous, Crystalline, Covalent Organic Frameworks. *Science (1979)* **2005**, *310* (5751), 1166−1170.
(12) Lohse, M. S.; Bein, T. Covalent Organic Frameworks: Structures, Synthesis, and Applications. *Adv. Funct Mater.* **2018**, *28* (33), 1705553.
(13) Huang, N.; Wang, P.; Jiang, D. Covalent Organic Frameworks: A Materials Platform for Structural and Functional Designs. *Nat. Rev. Mater.* **2016**, *1* (10), 16068.
(14) Zhu, D.; Zhu, Y.; Yan, Q.; Barnes, M.; Liu, F.; Yu, P.; Tseng, C. P.; Tjahjono, N.; Huang, P. C.; Rahman, M. M.; Egap, E.; Ajayan, P. M.; Verduzco, R. Pure Crystalline Covalent Organic Framework Aerogels. *Chem. Mater.* **2021**, *33* (11), 4216−4224.
(15) Alsudairy, Z.; Brown, N.; Yang, C.; Cai, S.; Akram, F.; Ambus, A.; Ingram, C.; Li, X. Facile Microwave-Assisted Synthesis of 2D Imine-Linked Covalent Organic Frameworks for Exceptional Iodine Capture. *Precision Chemistry* **2023**, *1* (4), 233−240.
(16) Brown, N.; Alsudairy, Z.; Behera, R.; Akram, F.; Chen, K.; Smith-Petty, K.; Motley, B.; Williams, S.; Huang, W.; Ingram, C.; Li, X. Green Mechanochemical Synthesis of Imine-Linked Covalent Organic Frameworks for High Iodine Capture. *Green Chem.* **2023**, *25* (16), 6287−6296.
(17) Zhu, D.; Xu, G.; Barnes, M.; Li, Y.; Tseng, C.; Zhang, Z.; Zhang, J.; Zhu, Y.; Khalil, S.; Rahman, M. M.; Verduzco, R.; Ajayan, P. M. Covalent Organic Frameworks for Batteries. *Adv. Funct Mater.* **2021**, *31*, 2100505.
(18) Wang, C.; Tang, J.; Chen, Z.; Jin, Y.; Liu, J.; Xu, H.; Wang, H.; He, X.; Zhang, Q. Ion-Selective Covalent Organic Frameworks Boosting Electrochemical Energy Storage and Conversion: A Review. *Energy Storage Mater.* **2023**, *55*, 498−516.
(19) Guo, J.; Jiang, D. Covalent Organic Frameworks for Heterogeneous Catalysis: Principle, Current Status, and Challenges. *ACS Cent Sci.* **2020**, *6* (6), 869−879.
(20) Lin, H.; Chen, C.; Zhou, T.; Zhang, J. Two-Dimensional Covalent-Organic Frameworks for Photocatalysis: The Critical Roles of Building Block and Linkage. *Solar RRL* **2021**, *5* (6), 2000458.
(21) Zhu, Y.; Zhu, D.; Chen, Y.; Yan, Q.; Liu, C.-Y.; Ling, K.; Liu, Y.; Lee, D.; Wu, X.; Senftle, T. P.; Verduzco, R. Porphyrin-Based Donor-Acceptor COFs as Efficient and Reusable Photocatalysts for PET-RAFT Polymerization under Broad Spectrum Excitation. *Chem. Sci.* **2021**, *12* (48), 16092−16099.
(22) Zhu, Y.; Liu, Y.; Ai, Q.; Gao, G.; Yuan, L.; Fang, Q.; Tian, X.; Zhang, X.; Egap, E.; Ajayan, P. M.; Lou, J. In Situ Synthesis of Lead-Free Halide Perovskite-COF Nanocomposites as Photocatalysts for Photoinduced Polymerization in Both Organic and Aqueous Phases. *ACS Mater. Lett.* **2022**, *4* (3), 464−471.
(23) Shi, Y.; Yang, J.; Gao, F.; Zhang, Q. Covalent Organic Frameworks: Recent Progress in Biomedical Applications. *ACS Nano* **2023**, *17* (3), 1879−1905.
(24) Fang, Q.; Pang, Z.; Ai, Q.; Liu, Y.; Zhai, T.; Steinbach, D.; Gao, G.; Zhu, Y.; Li, T.; Lou, J. Superior Mechanical Properties of Multilayer Covalent-Organic Frameworks Enabled by Rationally Tuning Molecular Interlayer Interactions. *Proc. Natl. Acad. Sci. U. S. A.* **2023**, *120* (15), e2208676120.
(25) Zhao, X.; Pachfule, P.; Thomas, A. Covalent Organic Frameworks (COFs) for Electrochemical Applications. *Chem. Soc. Rev.* **2021**, *50* (12), 6871−6913.
(26) Zhu, D.; Zhu, Y.; Chen, Y.; Yan, Q.; Wu, H.; Liu, C.-Y.; Wang, X.; Alemany, L. B.; Gao, G.; Senftle, T. P.; Peng, Y.; Wu, X.; Verduzco, R. Three-Dimensional Covalent Organic Frameworks with Pto and Mhq-z Topologies Based on Tri- and Tetratopic Linkers. *Nat. Commun.* **2023**, *14* (1), 2865.
(27) Beagle, L. K.; Moore, D. C.; Kim, G.; Tran, L. D.; Miesle, P.; Nguyen, C.; Fang, Q.; Kim, K.-H.; Prusnik, T. A.; Newburger, M.; Rao, R.; Lou, J.; Jariwala, D.; Baldwin, L. A.; Glavin, N. R. Microwave Facilitated Covalent Organic Framework/Transition Metal Dichalcogenide Heterostructures. *ACS Appl. Mater. Interfaces* **2022**, *14* (41), 46876−46883.
(28) Khaing, K. K.; Yin, D.; Ouyang, Y.; Xiao, S.; Liu, B.; Deng, L.; Li, L.; Guo, X.; Wang, J.; Liu, J.; Zhang, Y. Fabrication of 2D-2D Heterojunction Catalyst with Covalent Organic Framework (COF) and MoS2 for Highly Efficient Photocatalytic Degradation of Organic Pollutants. *Inorg. Chem.* **2020**, *59* (10), 6942−6952.
(29) Balch, H. B.; Evans, A. M.; Dasari, R. R.; Li, H.; Li, R.; Thomas, S.; Wang, D.; Bisbey, R. P.; Slicker, K.; Castano, I.; Xun, S.; Jiang, L.; Zhu, C.; Gianneschi, N.; Ralph, D. C.; Bredas, J.-L.; Marder, S. R.; Dichtel, W. R.; Wang, F. Electronically Coupled 2D Polymer/MoS2 Heterostructures. *J. Am. Chem. Soc.* **2020**, *142* (50), 21131−21139.
(30) Zhong, Y.; Cheng, B.; Park, C.; Ray, A.; Brown, S.; Mujid, F.; Lee, J. U.; Zhou, H.; Suh, J.; Lee, K. H.; Mannix, A. J.; Kang, K.; Sibener, S. J.; Muller, D. A.; Park, J. Wafer-Scale Synthesis of Monolayer Two-Dimensional Porphyrin Polymers for Hybrid Superlattices. *Science (1979)* **2019**, *366* (6471), 1379−1384.
(31) Sun, B.; Zhu, C.-H.; Liu, Y.; Wang, C.; Wan, L.-J.; Wang, D. Oriented Covalent Organic Framework Film on Graphene for Robust Ambipolar Vertical Organic Field-Effect Transistor. *Chem. Mater.* **2017**, *29* (10), 4367−4374.
(32) Sun, B.; Li, J.; Dong, W.-L.; Wu, M.-L.; Wang, D. Selective Growth of Covalent Organic Framework Ultrathin Films on Hexagonal Boron Nitride. *J. Phys. Chem. C* **2016**, *120* (27), 14706−14711.
(33) Lei, W.; Mochalin, V. N.; Liu, D.; Qin, S.; Gogotsi, Y.; Chen, Y. Boron Nitride Colloidal Solutions, Ultralight Aerogels and Free-standing Membranes through One-Step Exfoliation and Functionalization. *Nat. Commun.* **2015**, *6* (1), 8849.
(34) Wang, R.; Qian, J.; Chen, X.; Low, Z.-X.; Chen, Y.; Ma, H.; Wu, H.-A.; Doherty, C. M.; Acharya, D.; Xie, Z.; Hill, M. R.; Shen, W.; Wang, F.; Wang, H. Pyro-Layered Heterostructured Nanosheet Membrane for Hydrogen Separation. *Nat. Commun.* **2023**, *14* (1), 2161.
(35) Matsumoto, M.; Dasari, R. R.; Ji, W.; Feriante, C. H.; Parker, T. C.; Marder, S. R.; Dichtel, W. R. Rapid, Low Temperature Formation of Imine-Linked Covalent Organic Frameworks Catalyzed by Metal Triflates. *J. Am. Chem. Soc.* **2017**, *139* (14), 4999−5002.
(36) Matsumoto, M.; Valentino, L.; Stiehl, G. M.; Balch, H. B.; Corcos, A. R.; Wang, F.; Ralph, D. C.; Mariñas, B. J.; Dichtel, W. R. Lewis-Acid-Catalyzed Interfacial Polymerization of Covalent Organic Framework Films. *Chem.* **2018**, *4* (2), 308−317.
(37) Liu, Y.; Zhu, Y.; Alahakoon, S. B.; Egap, E. Synthesis of Imine-Based Covalent Organic Frameworks Catalyzed by Metal Halides and *in Situ* Growth of Perovskite@COF Composites. *ACS Mater. Lett.* **2020**, *2* (12), 1561−1566.
(38) Zhu, Y.; Zhang, J. Novel Catalysis Systems for the Synthesis of Covalent Organic Frameworks. *ChemistrySelect* **2023**, *8* (45), e202303959.
(39) Cai, W.; Hong, N.; Feng, X.; Zeng, W.; Shi, Y.; Zhang, Y.; Wang, B.; Hu, Y. A Facile Strategy to Simultaneously Exfoliate and Functionalize Boron Nitride Nanosheets via Lewis Acid-Base Interaction. *Chemical Engineering Journal* **2017**, *330*, 309−321.
(40) Zhang, Y.; Liu, T.; Xia, Q.; Jia, H.; Hong, X.; Liu, G. Tailoring of Surface Acidic Sites in Co-MoS2 Catalysts for Hydrodeoxygenation Reaction. *J. Phys. Chem. Lett.* **2021**, *12* (24), 5668−5674.
(41) Lei, Y.; Pakhira, S.; Fujisawa, K.; Liu, H.; Guerrero-Bermea, C.; Zhang, T.; Dasgupta, A.; Martinez, L. M.; Rao Singamaneni, S.; Wang, K.; Shallenberger, J.; Elías, A. L.; Cruz-Silva, R.; Endo, M.; Mendoza-Cortes, J. L.; Terrones, M. Low Temperature Activation of Inert Hexagonal Boron Nitride for Metal Deposition and Single Atom Catalysis. *Mater. Today* **2021**, *51*, 108−116.
(42) Feriante, C. H.; Jhulki, S.; Evans, A. M.; Dasari, R. R.; Slicker, K.; Dichtel, W. R.; Marder, S. R. Rapid Synthesis of High Surface Area Imine-Linked 2D Covalent Organic Frameworks by Avoiding Pore Collapse During Isolation. *Adv. Mater.* **2020**, *32* (2), 1905776.
(43) Mullangi, D.; Chakraborty, D.; Pradeep, A.; Koshti, V.; Vinod, C. P.; Panja, S.; Nair, S.; Vaidhyanathan, R. Highly Stable COF-

Supported Co/Co(OH)2 Nanoparticles Heterogeneous Catalyst for Reduction of Nitrile/Nitro Compounds under Mild Conditions. *Small* **2018**, *14* (37), 1801233.
(44) Ramalingam, A.; Samaraj, E.; Venkateshwaran, S.; Senthilkumar, S. M.; Senadi, G. C. 1T-MoS_2 Catalysed Reduction of Nitroarenes and a One-Pot Synthesis of Imines. *New J. Chem.* **2022**, *46* (18), 8720−8728.
(45) Wharf, I.; Gramstad, T.; Makhija, R.; Onyszchuk, M. Synthesis and Vibrational Spectra of Some Lead(II) Halide Adducts with O-, S-, and N-Donor Atom Ligands. *Can. J. Chem.* **1976**, *54* (21), 3430−3438.
(46) Zhu, Y.; Zhu, D.; Yan, Q.; Gao, G.; Xu, J.; Liu, Y.; Alahakoon, S. B.; Rahman, M. M.; Ajayan, P. M.; Egap, E.; Verduzco, R. Metal Oxide Catalysts for the Synthesis of Covalent Organic Frameworks and One-Step Preparation of Covalent Organic Framework-Based Composites. *Chem. Mater.* **2021**, *33* (15), 6158−6165.
(47) Liu, Y.; Zhou, W.; Teo, W. L.; Wang, K.; Zhang, L.; Zeng, Y.; Zhao, Y. Covalent-Organic-Framework-Based Composite Materials. *Chem.* **2020**, *6* (12), 3172−3202.
(48) Zhu, D.; Zhang, J. J.; Wu, X.; Yan, Q.; Liu, F.; Zhu, Y.; Gao, X.; Rahman, M. M.; Yakobson, B. I.; Ajayan, P. M.; Verduzco, R. Understanding Fragility and Engineering Activation Stability in Two-Dimensional Covalent Organic Frameworks. *Chem. Sci.* **2022**, *13* (33), 9655−9667.
(49) Qian, H. L.; Dai, C.; Yang, C. X.; Yan, X. P. High-Crystallinity Covalent Organic Framework with Dual Fluorescence Emissions and Its Ratiometric Sensing Application. *ACS Appl. Mater. Interfaces* **2017**, *9* (29), 24999−25005.
(50) Wang, K.; Jiang, H.; Liu, H.; Chen, H.; Zhang, F. Accelerated Direct Hydroxylation of Aryl Chlorides with Water to Phenols via the Proximity Effect in a Heterogeneous Metallaphotocatalyst. *ACS Catal.* **2022**, *12* (10), 6068−6080.
(51) Yang, J.; Ghosh, S.; Roeser, J.; Acharjya, A.; Penschke, C.; Tsutsui, Y.; Rabeah, J.; Wang, T.; Djoko Tameu, S. Y.; Ye, M.-Y.; Grüneberg, J.; Li, S.; Li, C.; Schomäcker, R.; Van De Krol, R.; Seki, S.; Saalfrank, P.; Thomas, A. Constitutional Isomerism of the Linkages in Donor-Acceptor Covalent Organic Frameworks and Its Impact on Photocatalysis. *Nat. Commun.* **2022**, *13* (1), 6317.
(52) Gan, S. X.; Jia, C.; Qi, Q. Y.; Zhao, X. A Facile and Scalable Synthetic Method for Covalent Organic Nanosheets: Ultrasonic Polycondensation and Photocatalytic Degradation of Organic Pollutants. *Chem. Sci.* **2022**, *13* (4), 1009−1015.
(53) Tan, F.; Zheng, Y.; Zhou, Z.; Wang, H.; Dong, X.; Yang, J.; Ou, Z.; Qi, H.; Liu, W.; Zheng, Z.; Chen, X. Aqueous Synthesis of Covalent Organic Frameworks as Photocatalysts for Hydrogen Peroxide Production. *CCS Chemistry* **2022**, *4* (12), 3751−3761.
(54) Coleman, J. N.; Lotya, M.; O'Neill, A.; Bergin, S. D.; King, P. J.; Khan, U.; Young, K.; Gaucher, A.; De, S.; Smith, R. J.; Shvets, I. V.; Arora, S. K.; Stanton, G.; Kim, H.-Y.; Lee, K.; Kim, G. T.; Duesberg, G. S.; Hallam, T.; Boland, J. J.; Wang, J. J.; Donegan, J. F.; Grunlan, J. C.; Moriarty, G.; Shmeliov, A.; Nicholls, R. J.; Perkins, J. M.; Grieveson, E. M.; Theuwissen, K.; McComb, D. W.; Nellist, P. D.; Nicolosi, V. Two-Dimensional Nanosheets Produced by Liquid Exfoliation of Layered Materials. *Science (1979)* **2011**, *331* (6017), 568−571.
(55) Zhu, L.; Su, Y.; Liu, Z.; Fang, Y. Shape-Controlled Synthesis of Covalent Organic Frameworks Enabled by Polymerization-Induced Phase Separation. *Small* **2023**, *19* (9), 2205501.
(56) Zhu, Y.; Liu, Y.; Miller, K. A.; Zhu, H.; Egap, E. Lead Halide Perovskite Nanocrystals as Photocatalysts for PET-RAFT Polymerization under Visible and Near-Infrared Irradiation. *ACS Macro Lett.* **2020**, *9* (5), 725−730.
(57) Wang, H.; He, B.; Liu, F.; Stevens, C.; Brady, M. A.; Cai, S.; Wang, C.; Russell, T. P.; Tan, T.-W.; Liu, Y. Orientation Transitions during the Growth of Imine Covalent Organic Framework Thin Films. *J. Mater. Chem. C Mater.* **2017**, *5* (21), 5090−5095.
(58) Zhao, W.; Yan, P.; Li, B.; Bahri, M.; Liu, L.; Zhou, X.; Clowes, R.; Browning, N. D.; Wu, Y.; Ward, J. W.; Cooper, A. I. Accelerated Synthesis and Discovery of Covalent Organic Framework Photocatalysts for Hydrogen Peroxide Production. *J. Am. Chem. Soc.* **2022**, *144* (22), 9902−9909.
(59) Smith, B. J.; Overholts, A. C.; Hwang, N.; Dichtel, W. R. Insight into the Crystallization of Amorphous Imine-Linked Polymer Networks to 2D Covalent Organic Frameworks. *Chem. Commun.* **2016**, *52* (18), 3690−3693.

https://doi.org/10.1021/prechem.3c00118
Precis. Chem. 2024, 2, 398−405